Characterization of Size and Aggregation for Cellulose Nanocrystal Dispersions Separated by Asymmetrical-Flow Field-Flow Fractionation

Maohui Chen,[a] Jeremie Parot [b], Arnab Mukherjee,[b] Martin Couillard,[a] Shan Zou, [a] Vincent A. Hackley,[b] and Linda J. Johnston[a]

[a] National Research Council Canada, Ottawa, ON, K1A 0R6, Canada

[b] National Institute of Standards and Technology, Gaithersburg, Maryland, 20899-8520, USA

Abstract

Cellulose nanocrystals (CNCs) derived from various types of cellulose biomass have significant potential for applications that take advantage of their availability from renewable natural resources and their high mechanical strength, biocompatibility and ease of modification. However, their high polydispersity and irregular rod-like shape present challenges for the quantitative dimensional determinations that are required for quality control of CNC production processes. Here we have fractionated a CNC certified reference material using a previously reported asymmetrical-flow field-flow fractionation (AF4) method and characterized selected fractions by atomic force microscopy (AFM) and transmission electron microscopy. This work was aimed at addressing discrepancies in length between fractionated and unfractionated CNC and obtaining less polydisperse samples with fewer aggregates to facilitate microscopy dimensional measurements. The results demonstrate that early fractions obtained from an analytical scale AF4 separation contain predominantly individual CNCs. The number of laterally aggregated "dimers" and clusters containing 3 or more particles increases with increasing fraction number. Size analysis of individual particles by AFM for the early fractions demonstrates that the measured CNC length increases with increasing fraction number, in good agreement with the rod length calculated from the AF4 multi-angle light scattering data. The ability to minimize aggregation and polydispersity for CNC samples has important implications for correlating data from different sizing methods.

Keywords

Cellulose nanocrystals, Asymmetrical-flow field-flow fractionation, Atomic force microscopy, Transmission electron microscopy

Electronic supplementary material

The online version of this article (https://doi xxxx) contains supplementary materials, which is available to authorized users.

Introduction

Cellulose nanomaterials have been the subject of increasing interest from both research scientists and industrial producers for the last decade (Klemm, Kramer et al. 2011, Dufresne 2013). This family of nanomaterials is derived from various types of cellulose biomass and their production from the world's most abundant biopolymer, their expected low toxicity and their novel properties make them candidates for a wide range of possible applications with significant commercial potential (Shatkin, Wegner et al. 2014, Jorfi and Foster 2015, Thomas, Raj et al. 2018, Dufresne 2019, Patel, Duttab et al. 2019, Wang 2019). Cellulose nanocrystals (CNCs) are typically generated by acid hydrolysis of larger fibrils, a process that in most cases leads to negatively charged surfaces decorated with, for example, sulfate half ester, carboxylate or phosphate groups (Eichhorn 2011, Moon, Martini et al. 2011, Brinchi, Cotana et al. 2013, Hamad 2014, Trache, Hussin et al. 2017). CNCs are rod-shaped particles with ~~high~~ typical aspect ratios of ≈~~≈~~20, high mechanical strength and low density. The negative surface groups lead to suspensions with high colloidal stability and facilitate surface modification to ensure compatibility with other materials. This range of properties makes CNCs promising candidates for applications as strengtheners for nanocomposites, rheology modifiers, additives for paints, thin films and food packaging and substrates for biomedical purposes (Eichhorn 2011, Dufresne 2013, Postek, Moon et al. 2013, Jorfi and Foster 2015).

As produced, CNCs typically have a wide size distribution, making particle size measurements challenging (Foster, Moon et al. 2018). For example, wood pulp CNCs have mean lengths and heights of (100 to 300) nm and (3 to 5) nm, respectively, with high polydispersity, as measured by atomic force microscopy (Moon, Martini et al. 2011, Brinkmann, Chen et al. 2016, Jakubek, Chen et al. 2018). It is also challenging to completely disperse CNC aggregates, even with extensive ultrasonication, due in part to their strong tendency to form ~~hydrogen bonded~~ lateral aggregates. The production of samples with narrower size distribution and minimal aggregation would be useful for assessing the impact of CNC morphology on properties that are important for applications, including their reinforcement capacity, rheological properties and self-assembly to generate chiral nematic films. The availability of samples with narrower size distributions may also be useful for nanotoxicology studies (Roman 2015, Shatkin and Kim 2015) and several separation procedures have been reported recently. ~~including d~~Differential centrifugation was used to separate CNCs produced by hydrolysis of microcrystalline cellulose; transmission electron microscopy (TEM) analysis demonstrated that fractions with a narrower length range (40 nm-160 nm) could be obtained from a sample with lengths up to 400 nm (Bai, Holberry et al. 2009). Phase separation of bacterial cellulose (Hirai, Inui et al. 2009) achieved separation into two layers with average CNC lengths of 800 and 1670 nm. ~~In both cases the initial CNCs were polydisperse with lengths up to 400 nm~~ (Bai, Holberry et al. 2009) ~~and 1500 nm~~ (Hirai, Inui et al. 2009) ~~and the extent of size fractionation was relatively low. An alternate~~A third approach using a multi-stage separation process with filter membranes ~~has shown that~~was used to fractionate CNCs with an initial high polydispersity (10-1700 nm length); the sample with the smallest CNCs was shown by TEM to have an average length and width that were reduced by a factor of two from those of the unfractionated sample (Hu and Abidi 2016). ~~can be partially fractionated and that~~Interestingly, the various fractions exhibited slightly different physical properties (Hu and Abidi 2016). All of

these examples used CNCs with relatively broad size distributions to facilitate the separation and none considered the effect of CNC aggregation on their results.

Recently several groups have reported on the use of asymmetrical-flow field-flow fractionation (AF4) in attempts to produce more monodisperse CNC samples (Guan, Cueto et al. 2012, Mukherjee and Hackley 2017, Ruiz-Palomero, Soriano et al. 2017). In one example, Guan and coworkers separated different fractions of CNC using AF4 with multi-angle light scattering (MALS) detection and compared their results to TEM of individual fractions (Guan, Cueto et al. 2012). The length calculated from the MALS data assuming a rod-like form factor agreed with the measured length from TEM for early fractions. A second study used AF4 to separate CNCs extracted from consumer products, demonstrating the possibility to obtain multiple fractions with calculated particle lengths between (30 and 110) nm (Ruiz-Palomero, Soriano et al. 2017), although there was no comparison with microscopy to validate the results. ~~Although~~ Some optimization of conditions was carried out in both of these studies but neither provided a detailed optimization of the various fractionation parameters or quantified the mass recovery, making it difficult to evaluate the results. In related work FFF was used to fractionate cellulose nanofibrils produced by free radical oxidation (Hiraoki, Tanaka et al. 2018). Nanofibrils with average lengths between (170 and 270) nm were adequately separated to give different size fractions and the distributions calculated in the FFF measurement matched the distribution obtained by TEM for the unfractionated sample. By contrast, nanofibrils with an average length > 400 nm could not be satisfactorily fractionated. The difficulty to achieve separation from longer fibrils may partially explain the rather poor fractionation attained in earlier studies using polydisperse CNCs with lengths in excess of 400 nm (Bai, Holberry et al. 2009, Hirai, Inui et al. 2009).

A detailed AF4 study from one of our groups focused on optimization of all parameters and demonstrated CNC fractionation with high mass recovery (> 95 %) for analytical separations (Mukherjee and Hackley 2017). These experiments utilized a combination of MALS, dynamic light scattering (DLS) and refractive index detection. Measurements of the radius of gyration and hydrodynamic diameter for each fraction gave shape factors in the range of 1.5 to 1.9, consistent with an elongated rod-like structure for the fractionated CNCs. Calculated rod lengths varied from approximately (104 to 204) nm, with a value of 146 nm at the AF4 peak maximum, considerably different from the previously reported mean lengths (Jakubek, Chen et al. 2018) for the same sample from either TEM (87 nm) or atomic force microscopy (AFM, 76 nm). Of particular interest, a semi-preparative method was also developed, opening the potential to produce larger amounts of fractionated CNC for research or applications (Mukherjee and Hackley 2017).

The~~se~~ previously optimized AF4 fractionation methods (Mukherjee and Hackley 2017) have been applied here to fractionate a CNC reference material that has been extensively characterized by DLS, AFM, TEM and static multiple light scattering in previous work (Brinkmann, Chen et al. 2016, Jakubek, Chen et al. 2018, Mazloumi, Johnston et al. 2018). This material is less polydisperse than some of the earlier studied samples, providing a better assessment of AF4 capabilities. Fractions were analyzed by both AFM and TEM, with a focus on correlating the AF4 data with microscopy measurements of particle size and aggregation level and providing an explanation for the discrepancies in CNC length observed in the previous AF4 study. The ~~results~~

~~demonstrate~~ early fractions from analytical AF4 separation are shown to contain predominantly individual CNCs with the number of laterally aggregated and clustered particles increasing substantially in later fractions. There is a modest increase in the mean length measured by AFM for individual particles in the first three AF4 fractions in reasonably good agreement with the lengths estimated from the MALS data. In addition to the separation achieved under optimized conditions the ability to eliminate almost all clusters from early fractions is an important observation. ~~that it is possible to obtain fractionated CNC samples that contain very few clusters, compared to the initial suspension prior to fractionation.~~ This indicates that the agglomeration and aggregation that is detected by microscopy probably reflects a combination of pre-existing aggregates in the initial suspension and clusters that form during the sample deposition process. ~~Although the early fractions contain predominantly individual CNCs, the number of laterally aggregated and clustered particles increase substantially in later fractions. There is a modest increase in the mean length measured by AFM for individual particles in the first three AF4 fractions in reasonably good agreement with the lengths estimated from the MALS data.~~

Materials and methods

Materials

CNC is a National Research Council Canada certified reference material (CNCD-1, www.nrc.ca/crm). The base material was produced by CelluForce Inc.,[1] Windsor QC by sulfuric acid hydrolysis of softwood pulp followed by neutralization and sodium exchange, purification and spray drying. CNC was dispersed at 2 % mass fraction in deionized water (Milli-Q, 18.2 MΩ cm at 25 °C) using a previously reported protocol (Jakubek, Chen et al. 2018). Suspensions were sonicated with a total energy of 5000 J/g (130 W Cole Parmer ultrasonic processor, EW-04714-50, with a ¼ inch probe) and stored at ≈ 5 ºC and diluted prior to use. The sonicator energy transfer efficiency was measured calorimetrically (Taurozzi, Hackley et al. 2011). The hydrodynamic diameter was measured by DLS (0.05 % mass fraction in 5 mmol L^{-1} NaCl) using a Zetasizer Nano ZS (Malvern Panalytical, Westborough, MA) to verify that the dispersion properties were consistent with previous reports (Jakubek, Chen et al. 2018).

Asymmetrical-flow field-flow fractionation

An Eclipse3+ (Wyatt Technology, Santa Barbara, CA) AF4 system was used for this study and coupled to a degasser (Gastorr TG-14, Flom Co., Ltd, Tokyo, Japan), an 1100-series isocratic pump (Agilent Technologies, Santa Clara, CA), a 1260 ALS series autosampler (Agilent Technologies), a MALS detector (Dawn Heleos-II, Wyatt Technology) with a laser at 661 nm and an online DLS detector at a scattering angle of 99.9° (Wyatt QELS, Wyatt Technology). Fractionation was conducted using a mobile phase ionic strength of 1 mmol L^{-1} NaCl.

[1] The identification of any commercial product or trade name does not imply endorsement or recommendation by the National Institute of Standards and Technology.

The optimized methods applied in this study used the parameters shown in Table 1. All on-line measurements were performed at 25 ± 0.1 °C, directly controlled by the MALS detector. Ambient temperature was within ± 2 °C of the experimentally controlled temperature. AF4 data was analyzed using OpenLab (Agilent Technologies) and Astra 6.1.7.17 (Wyatt Technology) software. DLS was used to measure the hydrodynamic radius and rod length was determined using the MALS data and rod model in the Astra software.

Three fractionated samples were prepared using semi-preparative and analytical separation conditions. A single fraction was collected for the semi-preparative methods and multiple fractions (numbered F1, F2, etc) were collected for the analytical separations. The details for each sample are summarized in Table 2.

Table 1 Parameters for semi-preparatory and analytical methods for AF4 fractionation of CNCs

		Semi-preparatory fractionation	**Analytical fractionation**
Channel type		Long channel	Long channel
Membrane		RC	RC
MWCO*		10 kDa	10 kDa
Spacer		490 µm	350 µm
Flow rates	Injection flow	0.2 mL min^{-1}	0.2 mL min^{-1}
	Detector flow	1.0 mL min^{-1}	0.5 mL min^{-1}
	Focus flow	2 mL min^{-1}	2 mL.min^{-1}
	Cross flow	0.2 mL min^{-1}	0.8 mL min^{-1}
Sample loading	Injected mass	2 mg	150 µg
Time parameters	(1) Elution	30 s	2 min
(as sequenced	(2) Focus	30 s	2 min
in the method)	(3) Focus + Injection	2 min	3 min
	(4) Focus	1min	3 min
	(5) Elution	10 min	60 min

* molecular weight cut-off, as defined by industry

Table 2 Summary of AF4 separation of CNCs

Sample	AF4 method	Fractions collected
B1	Semi-preparative	F25-40 nm
B2	analytical	F1, F2,…F7 (R_h from 22 to 70 nm
B3	analytical	F1, F2,…F10 (R_h from 20 to 75 nm)

Atomic force microscopy

The three AF4 fractionated samples were deposited on mica for AFM imaging. ~~studied by AFM: batch B1, prepared using semi-preparative conditions and batches B2 and B3 prepared by analytical separation. Fractions within each batch are numbered (e.g., F1, F2).~~ Most fractionated CNC suspensions were diluted to ≈ 0.001 % mass fraction with the exception of fractions B3-F4 to B3-F10, which had lower mass concentration and were not diluted. They were then vortex-mixed for 5 s, and spin-coated onto a mica substrate. A freshly cleaved mica substrate (2.54 cm × 2.54 cm) was first coated with 0.01 % mass fraction poly-L-lysine (PLL) solution (Sigma Aldrich, Oakville, ON) to provide a positively charged surface. A 200 µL aliquot of PLL solution was added onto the mica substrate, which was then covered with a petri dish for 10 minutes. The mica substrate was rinsed with deionized water five times and dried in a nitrogen stream. For spin coating, 200 µL (samples B1 and B2) or 100 µL (samples B3) of the freshly diluted CNC suspension was hand shaken for a few seconds and pipetted onto the center of a freshly prepared PLL-mica substrate, which was vacuum mounted onto a spin coater (WS-650SZ-6NPP/LITE, Laurel Technologies, North Wales, PA). The spin coating was performed immediately using static mode at 4000 rpm (66.7 Hz) and acceleration rate of 2000 rpm/s (33.3 Hz/s.).

The CNC-PLL-mica sample was mounted on a microscope slide for imaging with an AFM (NanoWizard II, JPK Instruments, Berlin, Germany). Intermittent contact mode was used with a silicon AFM tip (HQ:XSC11/AL BS, MikroMasch; typical radius 8 nm, 2.7 N/m spring constant). Large size images, (5 µm × 5 µm or 10 µm × 10 µm) were recorded to verify the overall morphology and homogeneity of the CNC samples. A series of small size AFM images was then acquired with 512 pixel × 512 pixel size, (0.8 to 1.0) Hz scan rate, and 1.5 µm Z-piezo range. To minimize compression of particles by the tip the ratio between the amplitude setpoint (A_{sp}) and the free amplitude (A_0) was set to ≈ 0.8–0.9. The AFM was calibrated using four step-height standards (VLSI Standards INC., STS3 series, 18 nm, 44 nm, 100 nm and 180 nm).

Images were flattened with a first-order polynomial fit using the JPK AFM software before processing using Gwyddion 2.45 (Czech Metrology Institute, Brno, Czech republic) for height and length analysis as outlined previously (Jakubek, Chen et al. 2018). For each image, all single particles were selected and their length and height measured. Particles adjacent to each other were only selected for analysis if the separation between the particles was clearly established in the contact or near-contact areas. Particles crossing or touching an edge of the image, particles < 25 nm long, particles crossing each other and particles with imaging artifacts were excluded. CNC length was measured by drawing a profile along the long axis of the particle and height was measured as the maximum value along the long axis, corrected for the background level where necessary.

To further investigate the effect of imaging force on the CNC height, some samples were imaged using a MultiMode AFM with a NanoScope V controller (Bruker Nano Surfaces Division, Santa Barbara, CA, USA), in PeakForce QNM® mode using PeakFroce Tapping® feedback control. Silicon nitride ScanAsyst-Air AFM probes (Bruker AFM Probes, Camarillo, CA, USA) were used in all PeakForce QNM® measurements. The manufacturer specified typical tip diameter and

spring constants are 2 nm and 0.4 N/m, respectively. In PeakForce Tapping® the force with which the tip periodically taps the surface is directly used as a feedback signal, meaning that the feedback loop keeps the peak force (maximum force between the tip and the sample) constant at a preselected value. This constant value is utilized to adjust the tip-sample positon, employing sinusoidal ramping function at each tap. The term force in Fig. 6 refers to this feedback peak force.

Transmission electron microscopy

Samples were prepared by diluting fractionated CNC suspension (fraction "B3-F1") to ≈ 0.001 % mass fraction with deionized water and depositing on plasma exposed (2 min, Model 1070, Fischione Instruments, Export, PA) carbon film covered copper grids (200 mesh, 01840-F, Ted Pella, Redding, CA). One drop of CNC suspension was deposited on the grid for 4 min and wicked with a filter paper. The sample was washed by adding one drop of deionized water to the grid and wicking with a filter paper after a few seconds. Finally, the sample was stained by depositing a drop of 2 % mass fraction uranyl acetate solution on the grid for 4 min and wicking away the solution with a wet filter paper. The grid was allowed to air dry before insertion into the microscope. Images were recorded with a Titan^3 80–300 (FEI, Thermo Fisher Scientific, Hillsbro, OR) transmission electron microscope operated at 300 kV and 27 k× magnification. The microscope calibration was verified by imaging a TEM magnification calibration standard (MAG*I*CAL, EMS).

TEM images were analyzed using a custom ImageJ (Rasband 2018) macro to measure the length and width of individual particles as described previously (Jakubek, Chen et al. 2018). Particles crossing one another were selected for analysis only if they crossed at an angle in the approximate range of 30° to 90° and there was a clear indication that the crossing particles can otherwise be considered as single CNCs. Those crossing at an angle outside the range specified above or adjacent to each other were selected for analysis only if the separation between the particles was clearly established in the contact areas.

Statistical analysis and uncertainties

Particle size distributions from AFM and TEM are reported as the arithmetic mean (length, height or width) and standard deviation as a measure of the spread of the distribution. Uncertainties are estimated as the 95 % confidence interval calculated from the standard error of the mean with a coverage factor of 2. Particle size distributions were compared using the two sample Kolmogorov-Smirnov test in Origin Pro 21018b. AF4 derived results (rod length or hydrodynamic radius) are reported as the mean and standard deviation of values measured continuously across the section of the peak corresponding to a specific fraction, where the standard deviation represents the spread in values within that fraction. Rod length should be considered as an estimate for examining trends, as the inherent uncertainty associated with the model is difficult to assess.

Results

CNC fractionation

A CNC suspension prepared from CNCD-1, an NRC reference material, was fractionated by AF4 using the semi-preparative method (sample B1, 2 mg injected mass) developed in earlier work (Mukherjee and Hackley 2017). A fraction with hydrodynamic radius (R_h) between (25 ± 0.5) nm and (40 ± 5) nm (B1 F25-40 nm) and a rod length average of (160 ± 80) nm was collected for microscopy analysis (Fig. 1A). CNCs were deposited on PLL-coated mica and imaged by AFM. Images showed a combination of individual and clustered CNCs (Fig. 1B), qualitatively similar to results obtained in earlier work for CNCD-1 and similar wood-pulp derived CNCs (Brinkmann, Chen et al. 2016, Jakubek, Chen et al. 2018). The length and height were measured for individual CNCs for a number of images; the mean length and height are summarized in Table 3~~2~~, with the standard deviation as a measure of the spread of the distributions, and histograms are shown in Fig. S1. The height distribution is not significantly different from that measured for CNCD-1 previously (see Table 2) based on comparison of the two distributions by Kolmogorov-Smirnov analysis (0.05 level); however, the length distributions for the fractionated sample and CNCD-1 are significantly different, consistent with the larger average length for the fractionated sample (Table ~~2~~3). Overall these results, and particularly the presence of a considerable fraction of clustered CNCs, indicate that collection of a relatively large fraction (based on retention time) near the maximum of the fractogram where the mass of recovered CNC is largest is not the best approach to obtain a CNC sample with a narrow size distribution and few aggregates/agglomerates.

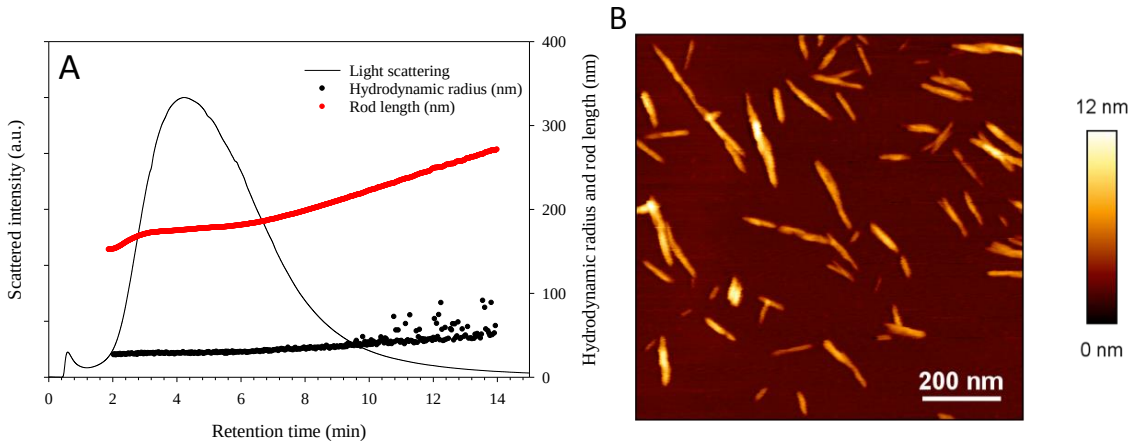

Fig. 1 AF4 fractogram of CNC obtained using semi-preparative conditions (A) and AFM image (B) of the fraction collected between (25 and 40) nm in hydrodynamic radius

A second AF4 fractionation experiment using the previously developed analytical method (see Table 1~~2~~) was carried out with injection of a smaller CNC mass (150 µg) and collection of 7 fractions (sample B2, F1-F7, 4 minute intervals) with R_h ranging from (22 ± 0.5) nm to (70 ± 2) nm and length from (104 ± 2) nm to (250 ± 5) nm (Fig. 2A). Fractions F1 to F7 were imaged; the

recovered mass decreased with increasing fraction number, requiring optimization of the sample dilution and deposition amounts to obtain an appropriate CNC density for imaging and collection of images on several different length scales. Representative AFM images for F1 and F4 are shown in Fig. 2B, C, clearly illustrating that the early fractions had a large number of individual CNCs, and very few clusters. By contrast the later fractions had predominantly clustered CNCs. Larger scale images (4 µm x 4 µm) were required in order to observe a reasonable number of particles for F6 and F7, which had very few CNCs. Multiple images for each fraction were analyzed by counting (1) individual CNCs, (2) features that are assigned to (two) laterally aggregated particles (dimers) and (3) clusters with 3 or more CNCs in more random orientations; the analysis procedure is illustrated with the cartoon in Fig. 2E. The results of this analysis are shown as a bar chart in Fig. 2D. Since it is difficult to distinguish single from laterally aggregated CNCs at the image scale used for fractions F6 and F7, singles and dimers were grouped together for these two fractions. Note that this analysis is qualitative since there are frequently several features/image that are challenging to assign to one of the three categories. However, the overall trend in the data is clear with clusters and dimers almost absent from fraction 1. Similar fractions of dimers are found in F2, F3 and F4, but the fraction of~~s~~ clusters increase~~s~~ ~~in the~~ at the expense of single CNCs.

Table 3~~2~~ Mean length and height/width data and uncertainty, along with the standard deviation as a measure of the distribution spread for unfractionated and fractionated CNC measured by AFM and TEM. Length estimated using a rod model for AF4-MALS data is also included for some fractions for samples B1 and B3 ~~fractions~~. Note that length and height were analyzed for only 3 fractions for sample B3 although the aggregation state was measured for all fractions (see Fig. 3).

Sample	Method (n)[a]	Length, nm		Height/width, nm	
		Mean[b]	Standard deviation[c]	Mean[b]	Standard deviation[c]
CNC, unfractionated[d]	AFM (1567)	76.3 ± 1.7	32.9	3.4 ± 0.1	1.1
CNC, unfractionated[e]	AFM (321)			3.5	1.1
CNC, unfractionated[d]	TEM (1909)	82 ± 2	36	7.5 ± 0.1	2.0
B1, F25-40 nm	AFM (234)	96 ± 5	39	3.5 ± 0.2	1.2
B1, F25-40 nm	AF4-MALS	160 ± 80			
B3, Fraction 1	AFM(240)	82 ± 4	30	3.2 ± 0.2	1.1
B3, Fraction 1	TEM (682)	73 ± 2	30	7.5 ± 0.1	1.8
B3, Fraction 1	AF4-MALS	113 ± 12	20		
B3, Fraction 2	AFM (227)	128 ± 4	44	3.9 ± 0.2	1.2
B3, Fraction 2	AF4-MALS	144 ± 8	15		
B3, Fraction 3	AFM (98)	138 ± 12	64	4.3 ± 0.3	1.4
B3, Fraction 3	AF4-MALS	166 ± 6	10		
B3, Fractions 1-3	AFM (564)	110 ± 4	50	3.7 ± 0.1	1.3

[a] n is the number of particles analyzed
[b] The uncertainty is the estimated 95% confidence interval for the calculated mean
[c] Standard deviation of the distribution as a measure of the distribution spread
[d] From Jakubek et al, 2018
[e] This work; measured using Peakforce AFM

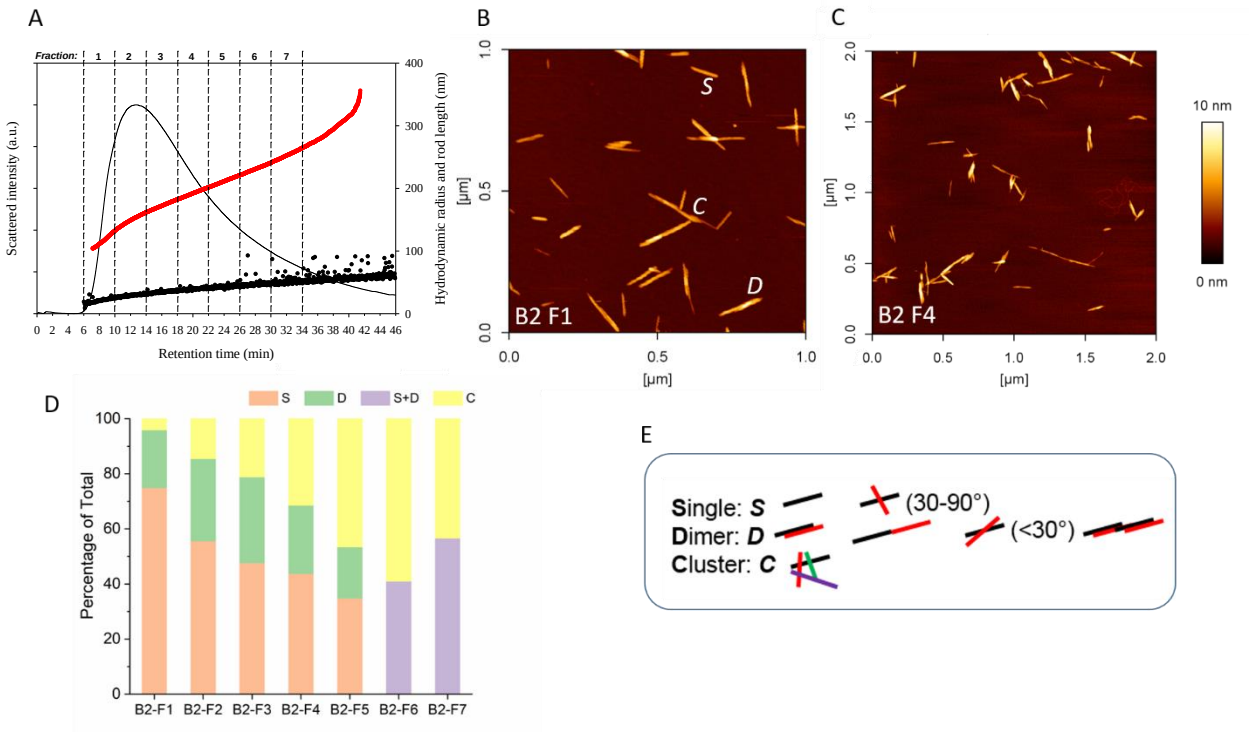

307

308 **Fig. 2** AF4 fractogram (A) for analytical separation of CNCs (sample B2) with AFM images of
309 fractions 1 and 4 (B, C). A qualitative illustration of the distribution of single, laterally aggregated
310 (dimers) and clustered CNCs is shown in the chart (D) with a cartoon (E) illustrating the
311 assignment of features in the AFM images. Single and dimer CNCs are grouped together for the
312 two last fractions in chart (D) since they cannot be unambiguously distinguished at the image
313 resolution used.

314

315 To test whether collection of narrower fractions provided an improvement in separation, an
316 additional experiment was carried out using the analytical method (Table 3~~2~~) with collection of 10
317 fractions (sample B3, F1 – F10) with R_h from (20 ± 0.5) nm to (75 ± 2) nm and rod length from
318 (97 ± 2) nm to (420 ± 35) nm (Fig. 3A). In this case, fractions were also collected at the highest
319 retention times where clusters are expected to predominate. Representative AFM images for the
320 various fractions are shown in Fig. 3B and C, Fig. S2 and S3. The same analysis procedure (see
321 Fig. 2E) was used to classify CNCs as singles, dimers or clusters. The results are shown as a bar
322 chart in Fig. 3D with singles and dimers also counted together for later fractions for which only
323 larger scale images were obtained. This sample exhibited the same overall trend as that shown in
324 Fig. 2, with predominantly single CNCs or dimers detected in the early fractions. However, this
325 sample yielded a smaller proportion of clustered CNCs in the later fractions, compared to the
326 results in Fig. 2. We attribute these differences to some combination of the following factors:
327 different elution times for the fractionation, variation in the numbers of particles counted and/or

differences in the AFM sample deposition procedure. Overall, there was a significant improvement in the fraction of single CNCs in the first 2 fractions when narrower fractions were collected.

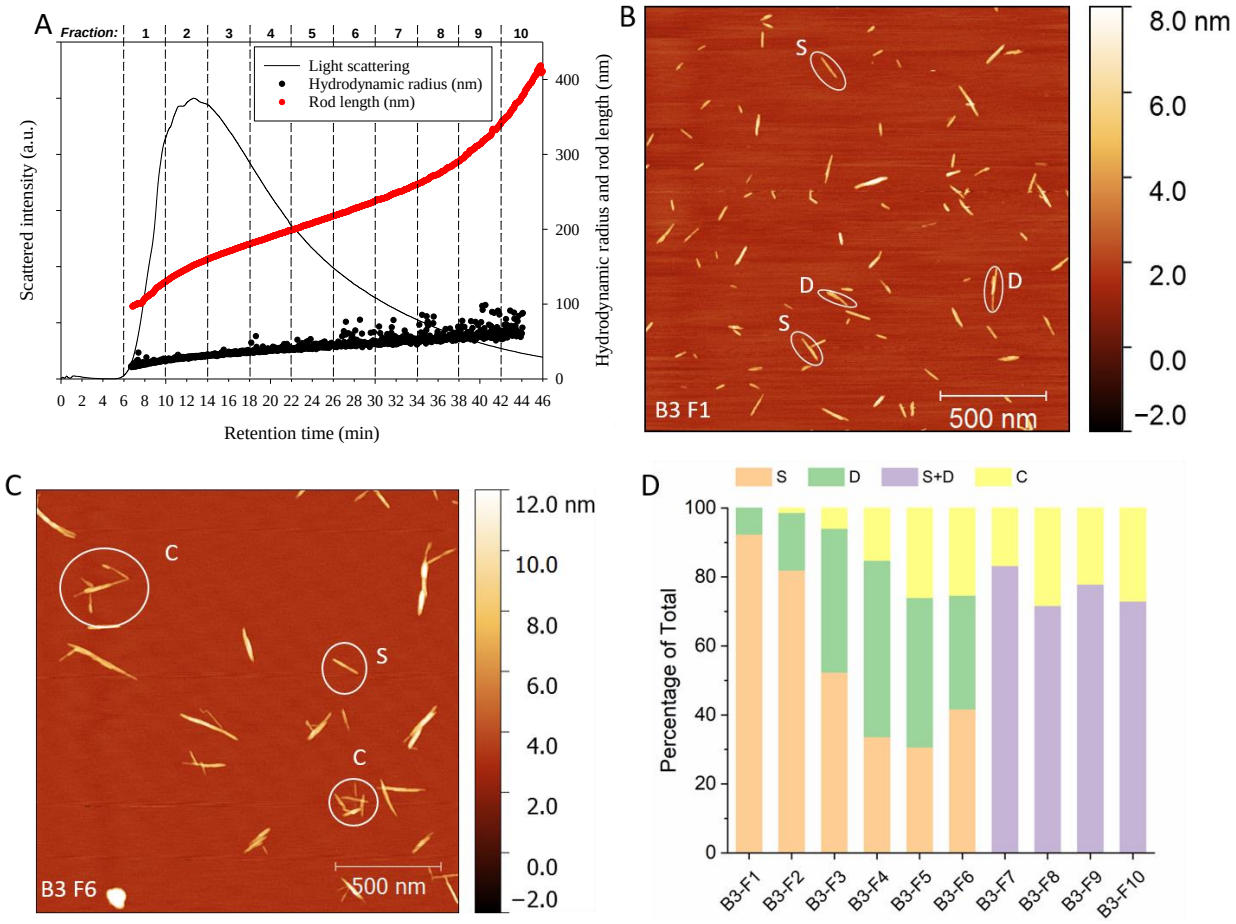

Fig. 3 AF4 fractogram (A) and AFM images for ~~selected~~ fractions F1 and F6 (B, C) from AF4 fractionation of CNC sample B3. Chart (D) shows a qualitative illustration of the distribution of single, dimer, and clustered CNCs

Particle size distributions for fractionated CNC

The height and length were measured for all individual CNCs in images collected for sample ~~(batch)~~ B3, fractions F1, F2 and F3, which had the highest numbers of individual CNCs. The AFM height and length distributions for each fraction are shown in Fig. 4; the mean values and their uncertainties and standard deviations as a measure of population spread are summarized in Table ~~2~~3. The length and height cumulative distributions for the sum of fractions F1 to F3 and the data for the unfractionated sample are provided for comparison. Kolmogorov-Smirnov analysis indicates that the three fractions each have different length distributions, consistent with the increase in average length with increasing fraction number. For height, F1 is different from both F2 and F3, which are not significantly different from each other at the 0.05 level. The cumulative

length and height distributions for each of the three fractions and for the combined F1, F2, F3 data set are all significantly different from the distributions for CNCD-1, although the data for the unfractionated CNCD-1 is based on a substantially larger data set corresponding to analysis of ≈ 300 CNCs for each of five independently prepared samples. Surprisingly the average length for each of the three fractions is larger than that measured for the unfractionated sample. Overall these results indicate that the population of individual CNCs analyzed for the fractionated sample differs from that in the unfractionated sample. It is likely that the AF4 separation is sensitive to overall size/dimensions, not just CNC length, consistent with the increase in clusters in later fractions; note that shape may also play a role in the separation process, as shown previously for separation of gold nanorods (Gigault, Cho et al. 2013). The AF4-MALS derived rod length estimates for the same B3 fractions are also listed in Table ~~2~~3; the AF4-MALS estimates for rod length are slightly larger than mean AFM lengths, but both MALS and AFM show the same trend of increasing length with increasing fraction number.

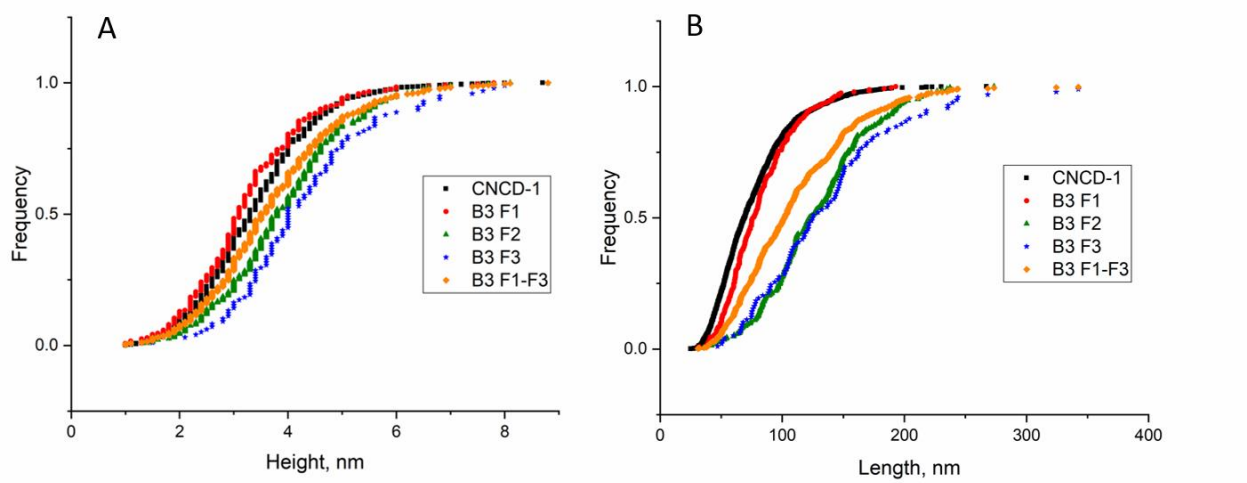

Fig. 4 Cumulative AFM distribution plots for CNC height (A) and length (B) for fractions F1, F2 and F3 from AF4 fractionation of sample B3. The distributions for the unfractionated sample (CNCD-1) and the combined (F1+F2+F3) data are also shown for comparison. The 3 fractions have different lengths and heights in all cases, except for height for F2 and F3. The combined data set (F1+F2+F3) differs from CNCD-1 for both length and height

Fraction 1 from the above experiment (B3) was also imaged by TEM for comparison to AFM data. Previous results for the unfractionated CNC sample had shown that the TEM width was approximately twice that of the AFM height (Jakubek, Chen et al. 2018). This result was somewhat surprising since models for CNCs derived from wood pulp have indicated that the CNC cross section has two axes with similar dimensions (Moon, Martini et al. 2011). The results were hypothesized to indicate a higher degree of lateral aggregation of CNCs after deposition for TEM and/or an inability to detect CNC aggregation by AFM due to tip convolution effects. TEM images for B3 F1 (Fig. 5A, B) showed that the fractionated sample gave better quality TEM images than

unfractionated CNC (see Fig. 7 in previous paper (Jakubek, Chen et al. 2018)), although there was still a higher proportion of CNC clusters (Fig. 5A, B) than is observed by AFM. The difference between AFM and TEM for the fractionated sample provides qualitative evidence that the TEM deposition and staining is responsible for at least some of the observed clusters. The length and width distributions for fraction 1 are different from those for unfractionated CNCD-1 (Fig. 5C, D and Table ~~2~~3), consistent with the AFM results. However, the average width for B3 F1 is still approximately twice the average AFM height, as observed previously for the unfractionated sample. Note that laterally aggregated CNCs are frequently observed in B3 F1 TEM images (Fig. S4), but these were not included in the size analysis to determine the width distribution. The length distribution is different as measured by AFM and TEM, which may indicate that the sample deposition process or grid-induced CNC clustering affects the measured CNC size distribution.

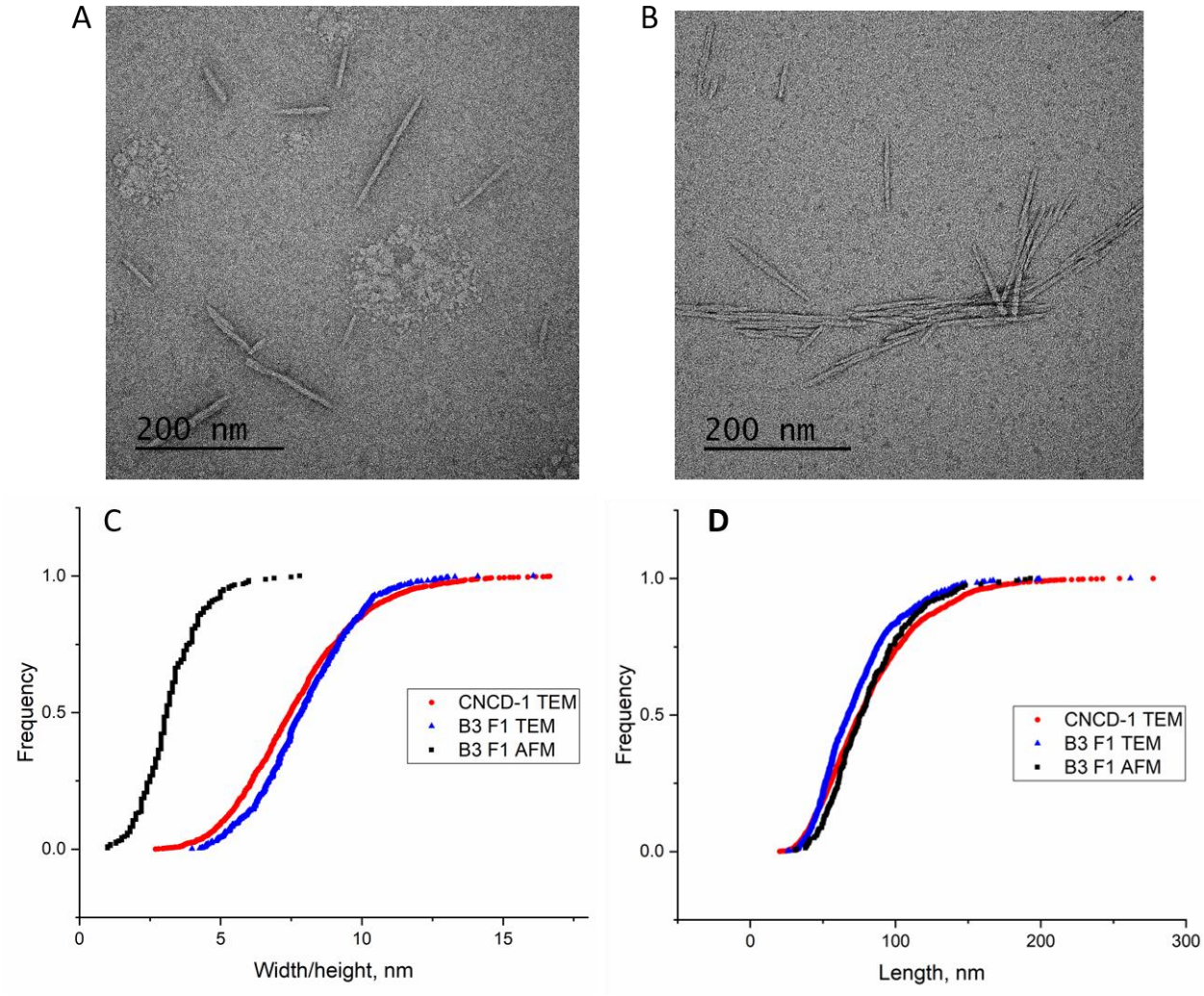

Fig. 5 TEM images (A, B) for sample B3, F1 with cumulative distributions for height (C) and length (D). The TEM size distributions are compared to the AFM distributions for F1 and the TEM distributions for the unfractionated sample (CNCD-1). Both length and height distributions are different for F1 and the unfractionated sample

Our previous study had considered the possibility that compression of the CNCs by the AFM tip might reduce the apparent CNC height and at least partially account for the difference between AFM height and TEM width (Jakubek, Chen et al. 2018). Based on the measured dependence of CNC height on applied force we concluded that compression by the tip due to the imaging setpoint used contributes 0.19 nm to the uncertainty in the measured height. Here we have further investigated this possibility by examining unfractionated CNC using PeakForce Tapping® AFM, which allows for imaging at much lower applied force. The results are summarized in Fig. 6 and demonstrate that CNCs can be imaged over a wide range of forces before the measured height decreases. For the experiment shown, the height starts to decrease above ≈ 500 pN and the image quality deteriorates above 2300 pN. This is dependent on the tip/experiment as thresholds for decreased heights of ≈ 1 nN were observed for replicate experiments using different tips. Analysis of multiple images obtained with an imaging force between (200 and 400) pN provided a mean CNC height of 3.5 nm with a standard deviation of 1.1 nm (n = 321, Table 3~~2~~) further support for the conclusion that compression of CNCs by the tip does not account for the factor of 2 difference between AFM height and TEM width.

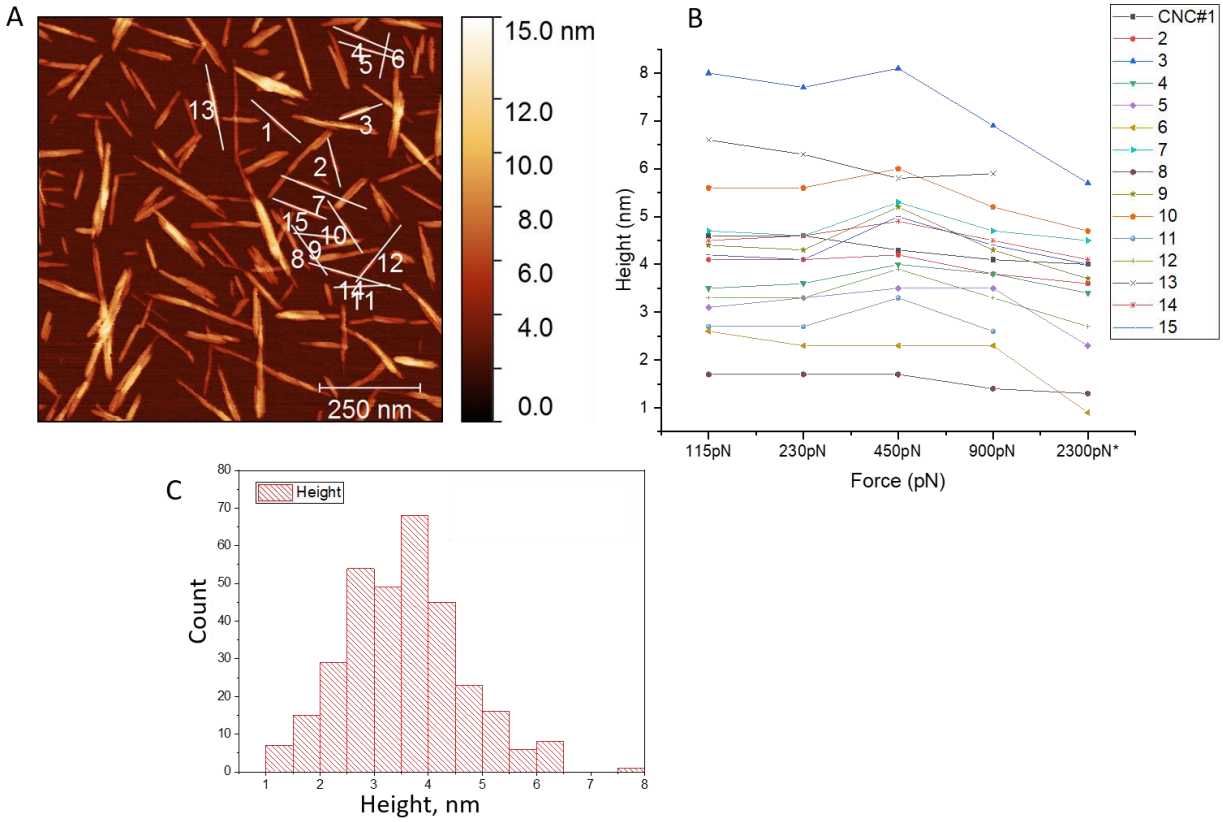

Fig. 6 AFM image of CNCD-1 using PeakForce Tapping® imaging (A). The plot of height vs. imaging force (B) shows the height for the particles marked with cross sections in (A). (C) Histogram of heights obtained by analyzing 321 CNCs

The AFM and TEM imaging results for fractionated CNC provides support for the hypothesis that some CNCs that appear as individual particles may be comprised of two laterally aggregated primary crystallites that are not distinguishable by either AFM or TEM. The crystallites may be linked by amorphous cellulose that is not removed during the acid hydrolysis or may be initially separated particles that are strongly hydrogen bonded. Recent experiments using small angle neutron scattering have concluded that several types of CNCs exhibit lateral aggregation that is dependent on concentration (Cherhal, Cousin et al. 2015, Uhlig, Fall et al. 2016). It has been suggested that two sides of crystalline cellulose are more polar than the other two; alignment of hydroxyl groups parallel to the crystalline plane results in a more polar surface compared to sides with hydroxyl groups oriented perpendicular to the crystalline plane. Interaction of the hydrophobic sides of two crystals will serve to expose the more hydrophilic surface to water, minimizing the free energy and providing a driving force for lateral aggregation (Uhlig, Fall et al. 2016). Experiments in which the height and width for identical CNCs can be reliably measured would be required to provide further insight into the presence and extent of lateral aggregation for the fractionated samples.

Discussion and Conclusions

As previously published, the AF4 approach has been developed and used for the analytical size-based separation of wood pulp derived CNCs (Mukherjee and Hackley 2017). In the present study the combination of AF4 with orthogonal techniques (i.e., AFM and TEM) permits us to explore the CNC composition of the fractions generated by this separation approach. AFM and TEM imaging results for AF4 fractionated CNCs highlight the capacity of this separation technique to isolate individual CNCs from larger clusters or aggregates. The first fraction contained predominantly individual CNCs with clusters of 3 or more CNCs increasing in number for all subsequent fractions. A significant number of features assigned to two laterally aggregated CNCs ("dimers") was observed in early fractions, but was lowest in the first fraction. Note that it was not possible to distinguish individual CNCs and dimers in later fractions which contained a low concentration of particles and required a lower image resolution in order to visualize a sufficient number of particles per image. It is noteworthy that CNC agglomeration/aggregation has so far been difficult, if not impossible, to avoid for CNC samples deposited for microscopy. The present study demonstrates clearly that it is possible to obtain AFM samples that contain predominantly individual CNCs, which dramatically improves the ability to measure size distributions. However, the separation method is so far compatible with preparation of relatively small amounts of material. It also appears from the data presented herein that one can minimize clustering using our spin coating method for deposition of AFM samples. The same does not apply to TEM where deposition and staining on the TEM grid leads to more CNC clustering than for CNCs on PLL-coated mica. Finally, the observation of clusters for later AF4 fractions (Fig 2 and 3) that have a low overall CNC mass provides clear evidence that these clusters are present in the initial suspension, and are not due to clustering that occurs during sample deposition and drying.

The use of AF4-MALS to evaluate the CNC rod length of CNC fractions (Table ~~2~~3) yields values that are similar to those obtained by microscopy for the early CNC fractions that are highly

enriched in individual particles. The later fractions as analyzed by AFM contain predominantly CNC clusters, which means that use of the rod model to obtain length from the MALS data is unlikely to be a suitable approach. The presence of a large fraction of clusters in later fractions therefore accounts for the lack of agreement between lengths obtained from microscopy and AF4-MALS data in the earlier study (Mukherjee and Hackley 2017). In that work a shape factor obtained as the ratio of R_g/R_h was shown to be approximately constant across the entire fractogram. However, it is likely that the measured shape factor is reliable for early fractions that do not contain a large number of clusters but possibly not for later fractions that contain a mixture of clusters with ill-defined morphology. It is also possible that the MALS results are dominated by local rod-like structure within clusters, and are not reflecting the larger scale cluster structure.

The present study has employed a less polydisperse CNC sample than some of the previous attempts at CNC fractionation using methods such as differential centrifugation, phase separation or separation on filter membranes (Bai, Holberry et al. 2009, Hirai, Inui et al. 2009, Hu and Abidi 2016). Our results indicate that AF4 fractionation is possible for a less polydisperse CNC sample, indicating that it may be a more generally useful method. One previous AF4 study demonstrated separation of CNCs in commercial samples, a useful result, but not directly comparable to our work since AF4 was not correlated with an orthogonal method and the initial CNC size distribution was unknown. In related work, AF4 fractions were assessed by TEM and the extent of size fractionation (rod lengths of approximately 85 and 105 for fractions 1 and 3 from MALS) for microcrystalline cellulose CNC was similar to that shown in Table 3. There was good agreement between TEM and MALS data for early fractions but a larger difference between methods for the later fractions, similarly to what we observe here. Our correlation of AF4 data with TEM indicates that later fractions contain predominantly aggregated CNCs, a factor that was not considered in the previous study. The present study has the additional advantage of optimized AF4 conditions to achieve high mass recovery.

Future work should be directed towards improvement in preparative methodology for higher throughput with narrow size fractions. Examining the laterally aggregated “dimers” as a function of AF4 parameters such as focus flow and time, or crossflow could be used to test whether some of the observed clusters in the later fractions may be created during the AF4 experiment. Note however, that the measured R_h of 22 nm for the first fraction (B3 F1) is approximately 1.5 times lower than that for the unfractionated CNC (≈ 35 nm) which presumably is mostly due to the presence of CNC clusters in the unfractionated sample; note that larger clusters may dominate the intensity-based DLS results. Additional microscopy experiments aimed at measuring both length and height for the same CNC entities would be useful to confirm hypotheses from this and earlier work. The availability of fractionated samples with low numbers of clusters is an important prerequisite for such experiments.

Acknowledgments

We thank Valerie Bartlett (NRC) for analysis of TEM images and Zygmunt Jakubek (NRC) for advice on use of a custom ImageJ macro for TEM image analysis. We thank Tae Joon Cho and Natalia Farkas (NIST) for helpful comments on the manuscript.

References

Bai, W., J. Holberry and K. Li (2009). "A technique for production of nanocrystalline cellulose with a narrow size distribution." Cellulose **16**: 455-465.

Brinchi, L., F. Cotana, E. Fortunati and J. M. Kenney (2013). "Production of nanocrystalline cellulose from lignocellulosic biomass: technology and applications." Carbohy. Poly. **94**: 154-169.

Brinkmann, A., M. Chen, M. Couillard, Z. J. Jakubek, T. Leng and L. J. Johnston (2016). "Correlating cellulose nanocrystal particle size and surface area " Langmuir **32**: 6105-6114.

Cherhal, F., F. Cousin and I. Capron (2015). "Influence of charge density and ionic strength on the aggregation process of cellulose nanocrystals in aqueous suspension, as revealed by small-angle neutron scattering." Langmuir **31**: 5596-5602.

Dufresne, A. (2013). "Nanocellulose: a new ageless bionanomaterial." Materials Today **16**: 220-227.

Dufresne, A. (2019). "Nanocellulose processing properties and potential applications." Current Forestry Reports **5**: 76-89.

Eichhorn, S. (2011). "Cellulose nanowhiskers: Promising materials for advanced applications." Soft Matter **7**: 303-315.

Foster, E. J., R. J. Moon, U. P. Agarwal, M. J. Bortner, J. Bras, S. Camarero-Espinosa, K. J. Chen, M. J. D. Clift, E. D. Cranston, S. J. Eichhorn, D. M. Fox, W. Y. Hamad, L. Heux, B. Jean, M. Korey, W. Nieh, K. J. Ong, M. S. Reid, S. Renneckar, R. Roberts, J. A. Shatkin, J. Simonsen, K. Stinson-Bagby, N. Wanasekara and J. Youngblood (2018). "Current characterization methods for cellulose nanomaterials." Chem. Soc. Rev. **47**: 2609-2679.

Gigault, J., T. J. Cho, R. I. MacCuspie and V. A. Hackley (2013). "Gold nanorod separation and characterization by asymmetric-flow field flow fractionation with UV-vis detection." Anal. Bioanal. Chem. **405**: 1191-1202.

Guan, X., R. Cueto, P. Russo, Y. Qi and Q. Wu (2012). "Asymmetric flow field-flow fractionation with multiangle light scattering detection for characterization of cellulose nanocrystals " Biomacromolecules **13**: 2671-2679.

Hamad, W. Y. (2014). "Development and properties of nanocrystalline cellulose." ACS Symp. Ser. **1067**: 301-321.

Hirai, A., O. Inui, F. Horii and M. Tsuji (2009). "Phase separation behavior in aqueous suspensions of bacterial cellulose nanocrystals prepared by sulfuric acid treatment." Langmuir **25**: 497-502.

Hiraoki, R., R. Tanaka, Y. Ono, M. Nakamura, T. Isogai, T. Saito and A. Isogai (2018). "Determination of length distribution of TEMPO-oxidized cellulose nanofibrils by field-flow fractionation/multi-angle laser-light scattering analysis." Cellulose **25**: 1599-1606.

Hu, Y. and N. Abidi (2016). "Distinct nematic self-assembling behavior caused by different size-unified cellulose nanocrystals via a multistage separation." Langmuir **32**: 9863-9872.

Jakubek, Z. J., M. Chen, M. Couillard, T. Leng, L. Liu, S. Zou, U. Baxa, J. D. Clogston, W. Hamad and L. J. Johnston (2018). "Characterization challenges for a cellulose nanocrystal reference material: Dispersion and particle size distributions " J. Nanopart. Res. **20**: 98.

Jorfi, M. and E. J. Foster (2015). "Recent advances in nanocellulose for biomedical applications." J. Appl. Polym. Sci. **2015**: 41719.

Klemm, D., F. Kramer, S. Moritz, T. Lindstrom, M. Ankerfors, D. Gray and A. Dorris (2011). "Nanocelluloses: A new family of nature-based materials." Angew. Chem. Int. Ed. Engl. **50**: 5438-5466.

Mazloumi, M., L. J. Johnston and Z. J. Jakubek (2018). "Dispersion, stability and size measurements for cellulose nanocrystals by static multiple light scattering." Cellulose **25**: 5751-5768.

Moon, R. J., A. Martini, J. Nairn, J. Simonsen and J. Youngblood (2011). "Cellulose nanomaterials review: structure, properties and nanocomposites." Chem. Soc. Rev. **40**: 3941-3994.

Mukherjee, A. and V. A. Hackley (2017). "Separation and characterization of cellulose nanocrystals by multi-detector asymmetric flow field-flow fractionation." Analyst **143**: 731-740.
Patel, D. K., S. D. Duttab and K.-Y. Lim (2019). "Nanocellulose-based polymer hybrids and their emerging applications in biomedical engineering and water purification." RSC Adv. **9**: 19143-19162.
Postek, M. T., R. J. Moon, A. W. Rudie and M. A. Bilodeau, Eds. (2013). Production and applications of cellulose nanomaterials. Atlanta, GA, TAPPI Press.
Rasband, W. S. (2018). "ImageJ." from https://imagej.nih.gov/ij/.
Roman, M. (2015). "Toxicity of cellulose nanocrystals: a review." Industrial Biotech. **11**: 25-33.
Ruiz-Palomero, C., M. L. Soriano and M. Valcarcel (2017). "Detection of nanocellulose in commercial products and its size characterization using asymmetric flow field-flow fractionation." Microchim. Acta **184**: 1069-1076.
Shatkin, J. A. and B. Kim (2015). "Cellulose nanomaterials: life cycle risk assessment and environmental health and safety roadmap." Environ. Sci.: Nano **2**: 477-499.
Shatkin, J. A., T. H. Wegner, E. M. Bilek and J. Cowie (2014). "Market projections of cellulose nanomaterial-enabled products- Part 1: Applications." TAPPI J. **13**: 9-16.
Taurozzi, J. S., V. A. Hackley and M. R. Wiesner (2011). "Ultrasonic dispersion of nanoparticles for environmental, health and safety assessment - issues and recommendations." Nanotoxicology **5**: 711-729.
Thomas, B., M. C. Raj, K. B. Athira, M. H. Rubiyah, J. Joy, A. Moores, G. L. Drisko and C. Sanchez (2018). "Nanocellulose, a versatile green platform: from biosources to materials and their applications." Chem. Rev. **118**: 11575-11625.
Trache, D., M. H. Hussin, M. K. M. Haafiz and V. K. Thakur (2017). "Recent progress in cellulose nanocrystals: sources and production." Nanoscale **9**: 1763-1786.
Uhlig, M., A. Fall, S. Wellert, M. Lehmann, S. Prévost, L. Wågberg, R. von Klitzing and G. Nyström (2016). "Two-Dimensional Aggregation and Semidilute Ordering in Cellulose Nanocrystals." Langmuir **32**: 442-450.
Wang, D. (2019). "A critical review of cellulose-based nanomaterials for water purification in industrial processes." Cellulose **26**: 687-701.

Electronic Supplementary Material

Characterization of Size and Aggregation for CNC Dispersions Separated by Asymmetrical-flow Field-flow Fractionation

Maohui Chen,[a] Jeremie Parot [b], Arnab Mukherjee,[b] Martin Couillard,[a] Shan Zou, [a] Vincent A. Hackley,[b] and Linda J. Johnston[a]

[a] National Research Council Canada, Ottawa, ON, K1A 0R6, Canada

[b] National Institute of Standards and Technology, Gaithersburg, Maryland, 20899-8520, USA

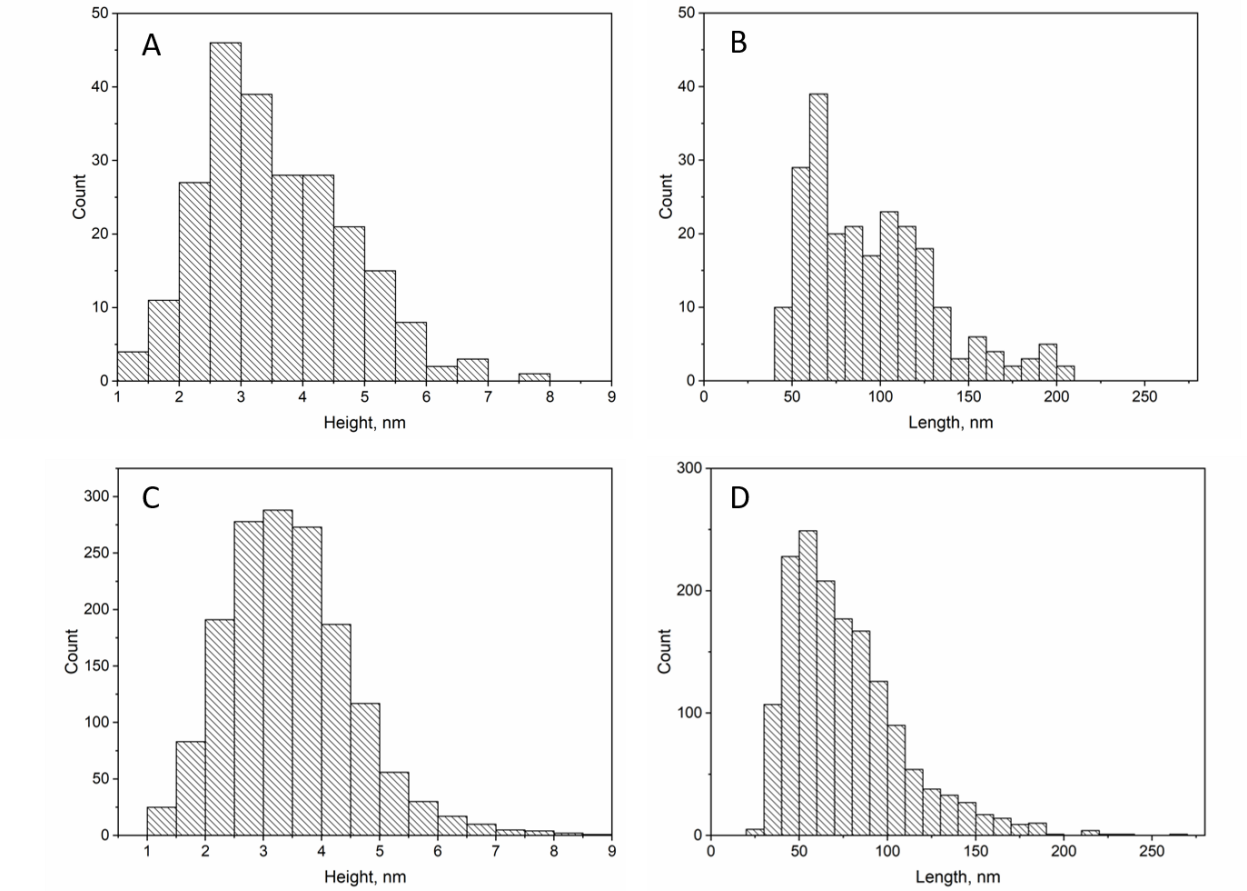

Fig. S1 Histograms for AFM measured height and length for fractionated CNC (sample B1, F25-40 nm, A, B) and the original unfractionated CNC (CNCD-1, C, D). The length distributions are different for the two samples, but the height distributions are not significantly different (Kolmogorov-Smirnov test, 0.05 level). Data for CNCD-1 is from Jakubek et al, 2018; note that the bin size for histograms C and D has been changed for ease of comparison to the fractionated sample.

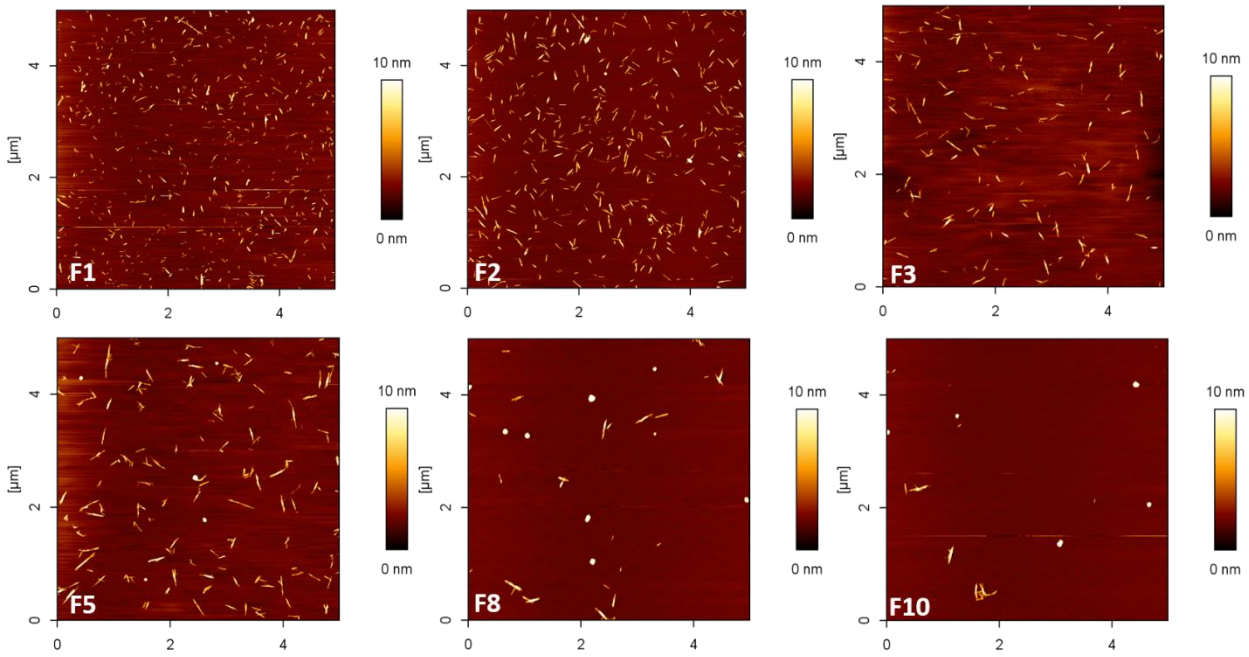

Fig. S2 Representative AFM images for selected fractions for sample B3. Images are all on the same scale for ease of visualization of the change in CNC density

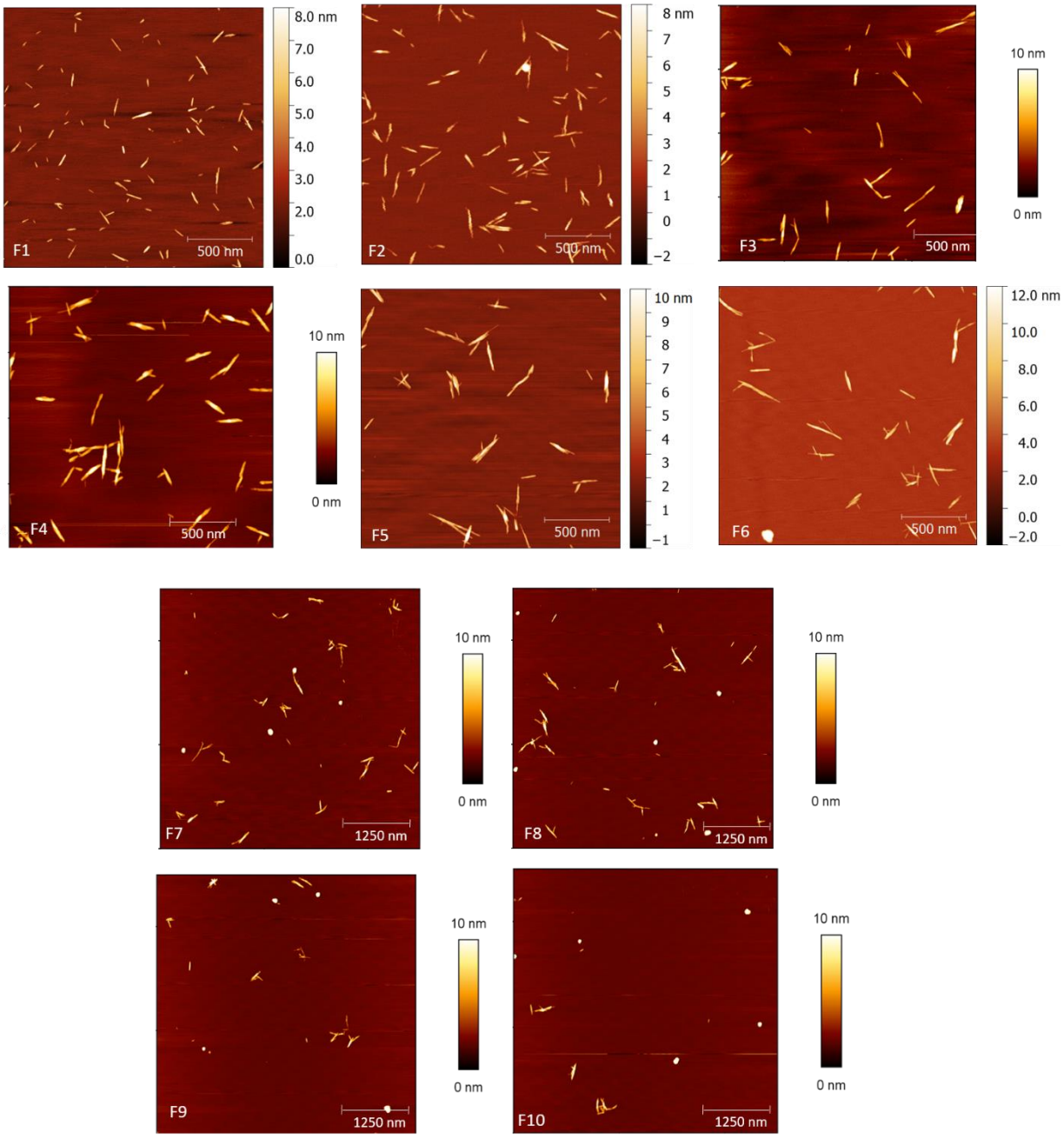

Fig. S3 Representative AFM images for all fractions for sample B3. Images are shown on different length scales in order to visualize individual and clustered particles

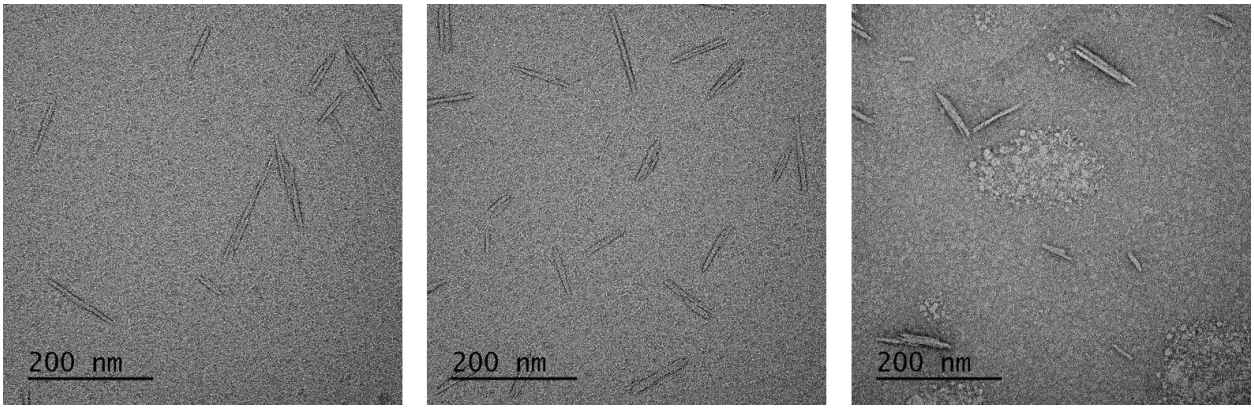

Fig. S4 Additional TEM images for fractionated sample B3 F1 illustrating the ability to distinguish two laterally aggregated CNCs.

Reference

Jakubek ZJ, Chen M, Couillard M, Leng T, Liu L, Zou S, Baxa U, Clogston JD, Hamad W, Johnston LJ (2018) Characterization challenges for a cellulose nanocrystal reference material: Dispersion and particle size distributions J. Nanopart. Res., 20:98.